



**QUEEN'S
UNIVERSITY
BELFAST**

Modeling microplastic and solute transport in vegetated flows

Stride, B., Abolfathi, S., Odara, M. G. N., Bending, G. D., & Pearson, J. (2023). Modeling microplastic and solute transport in vegetated flows. *Water Resources Research*, 59(5), Article e2023WR034653. <https://doi.org/10.1029/2023WR034653>

Published in:

Water Resources Research

Document Version:

Publisher's PDF, also known as Version of record

Queen's University Belfast - Research Portal:

[Link to publication record in Queen's University Belfast Research Portal](#)

Publisher rights

Copyright 2024 the authors.

This is an open access article published under a Creative Commons Attribution License (<https://creativecommons.org/licenses/by/4.0/>), which permits unrestricted use, distribution and reproduction in any medium, provided the author and source are cited.

General rights

Copyright for the publications made accessible via the Queen's University Belfast Research Portal is retained by the author(s) and / or other copyright owners and it is a condition of accessing these publications that users recognise and abide by the legal requirements associated with these rights.

Take down policy

The Research Portal is Queen's institutional repository that provides access to Queen's research output. Every effort has been made to ensure that content in the Research Portal does not infringe any person's rights, or applicable UK laws. If you discover content in the Research Portal that you believe breaches copyright or violates any law, please contact openaccess@qub.ac.uk.

Open Access

This research has been made openly available by Queen's academics and its Open Research team. We would love to hear how access to this research benefits you. – Share your feedback with us: <http://go.qub.ac.uk/oa-feedback>






Water Resources Research®



RESEARCH ARTICLE

10.1029/2023WR034653

Modeling Microplastic and Solute Transport in Vegetated Flows

Ben Stride¹ , Soroush Abolfathi¹ , M. G. N. Odara¹ , Gary D. Bending² , and Jonathan Pearson¹ 

¹School of Engineering, University of Warwick, Coventry, UK, ²School of Life Sciences, University of Warwick, Coventry, UK

Key Points:

- Neutrally buoyant microplastics disperse analogous to solutes within the water column of fluvial environments with submerged vegetation
- A novel fluorometric tracing and particle staining technique is proven to accurately trace stained microplastics within vegetated flows
- A robust hydrodynamic model is proven to predict mixing of neutrally buoyant microplastics

Supporting Information:

Supporting Information may be found in the online version of this article.

Correspondence to:

B. Stride,
ben.stride@warwick.ac.uk

Citation:

Stride, B., Abolfathi, S., Odara, M. G. N., Bending, G. D., & Pearson, J. (2023). Modeling microplastic and solute transport in vegetated flows. *Water Resources Research*, 59, e2023WR034653. <https://doi.org/10.1029/2023WR034653>

Received 12 FEB 2023
Accepted 28 APR 2023

Author Contributions:

Conceptualization: Ben Stride, M. G. N. Odara, Jonathan Pearson
Investigation: Ben Stride, Soroush Abolfathi, Jonathan Pearson
Methodology: Ben Stride, M. G. N. Odara, Jonathan Pearson
Resources: Ben Stride
Supervision: Soroush Abolfathi, Gary D. Bending, Jonathan Pearson
Visualization: Ben Stride, Soroush Abolfathi
Writing – original draft: Ben Stride
Writing – review & editing: Ben Stride, Soroush Abolfathi, Gary D. Bending, Jonathan Pearson

© 2023. The Authors.

This is an open access article under the terms of the [Creative Commons Attribution License](https://creativecommons.org/licenses/by/4.0/), which permits use, distribution and reproduction in any medium, provided the original work is properly cited.

Abstract Physical interactions of microplastics within vegetation and turbulent flows of freshwater systems are poorly understood. An experimental study was conducted to investigate the underlying physical transport mechanisms of microplastics over submerged canopies across a range of flow conditions common in the natural environment. The effects of changing canopy heights were investigated by testing two model canopies of varying stem heights, simulating seasonal variation. This study determined and compared the mixing and dispersion processes for microplastics and solutes utilizing fluorometric tracing techniques. A hydrodynamic model was developed based on the advection-dispersion equation for quantifying microplastic mixing in submerged canopies. Longitudinal dispersion coefficients for neutrally buoyant microplastics (polyethylene) and solutes were significantly correlated within submerged model vegetation irrespective of the complexity of the flow regime. Hydrodynamic and solute transport models were shown to be capable of robust predictions of mixing for neutrally buoyant microplastics in environmental flows over a canopy, facilitating a new approach to quantify microplastic transport and fate. We compare the mixing processes for microplastics and solutes then propose a hydrodynamic model for quantifying the mixing in submerged canopies.

Plain Language Summary Microplastic movement and fate within vegetation and turbulent flows of freshwater systems is poorly understood. A study was conducted within a laboratory flume, scaled for real-world river systems, to investigate the transport of microplastics over submerged canopies across a range of flow conditions common in the natural environment. The effects of changing vegetation heights were investigated by testing two model canopies of varying stem heights, simulating seasonal variation. To measure microplastic movement in real-time this study determined and compared the mixing of microplastics and solutes using fluorometric techniques that measure fluorescence at specific wavelengths of light produced by the stained microplastics and Rhodamine WT dye (solute). Models utilizing velocities over depth and solute dispersion were adapted to quantify microplastic mixing in submerged canopies. The dispersion of neutrally buoyant microplastics (polyethylene), microplastics of a similar buoyancy to water, and solutes were significantly correlated within submerged vegetation irrespective of the complexity of the flow regime. The models were shown to be capable of reliable predictions of mixing for neutrally buoyant microplastics in environmental flows over a canopy, facilitating a new approach to measure microplastic transport and fate.

1. Introduction

Over 5 trillion tonnes of plastic are afloat at sea (Eriksen et al., 2014) and up to 80% of plastics enter the ocean through river networks (Ockelford et al., 2020) causing potential long-term effects on ecosystems and ecosystem function. Detailed understanding of the underlying physical mechanisms that govern the behavior, transport, and fate of plastics is needed to assess their impact on freshwater systems with complex flows (Abolfathi et al., 2020; Anderson et al., 2016; Bucci et al., 2020; Dris et al., 2018; Wagner et al., 2014). Plastic pollution is not only a concern because of the sheer volume being discarded, but because plastic polymers such as polyethylene (PE), polypropylene (PP), polystyrene (PS), and polyvinyl chloride (PVC) are so resistant to degradation. These polymers can persist in the environment for centuries, enabling them to be transported far from their original source and often ending up in aquatic systems. Recent studies have shown plastics being found in the remotest of regions, including the six deepest ecosystems on earth (Jamieson et al., 2019) and sea ice in the Arctic (Peeken et al., 2018). When plastics do degrade, they break off in fragments from larger plastic objects and when smaller than 5 mm and larger than 1 μm, plastic polymer fragments are defined as microplastics (Frias & Nash, 2019). There are many pathways microplastics can take to enter riverine ecosystems, from waste-water

inputs to groundwater leaching, surface run-off, inappropriate waste management, and atmospheric deposition (Allen et al., 2019; Barnes et al., 2009; Horton et al., 2017; Klemeš et al., 2020; Talsness et al., 2009). PE, PS, PP, and PVC from tyres and road wear, along with abraded plastics from textiles during laundry, and broken-down packaging account for most of the plastic polymers transported by rivers in Europe (Bråte et al., 2014; Horton et al., 2017; Rowley et al., 2020; Siegfried et al., 2017). Smaller sized plastics are considered a greater threat to humans and the environment (Edo et al., 2020) due to being easily ingested and significantly more abundant than large plastic particles (Erni-Cassola et al., 2017). Long-term effects of microplastic ingestion on human health are not fully understood but microplastics have recently been shown to accumulate in digestive tracts, blood streams, and lungs in humans (Jenner et al., 2022; Leslie et al., 2022; Miller et al., 2020; Sana et al., 2020).

Existing numerical models cannot robustly simulate the transport of microplastics in fluvial systems as there is limited physical modeling data to validate and calibrate such models. Solute transport models based upon the advection-dispersion equation have been meticulously developed (e.g., Elder, 1958; Fischer, 1966; Rutherford, 1994; Taylor, 1954) and are widely validated for tracer measurements across a wide range of flow domains including pipes, laboratory flumes, and natural rivers (e.g., Abolfathi & Pearson, 2017; Jimoh & Abolfathi, 2022). Thus, these models provide a suitable foundation to quantify the transport processes which govern pollution behavior. Such models could also provide accurate approximations for the transport and dispersion of microplastics that have a similar density to solutes and are below 0.2 mm in size (see Section 4.3), where the assumption of a vertically well-mixed plume is valid. Most PE and PS particles have near neutral buoyancies of between 0.91 and 0.97 g/cm³ and 1.05 g/cm³ respectively (van Emmerik & Schwarz, 2019), indicating they may follow the same transport pathways as solutes in turbulent flow systems governed by advection or turbulence in the natural environment. For a specific size range and shape PE-particles can behave analogous to conservative solutes such as Rhodamine WT for open channel flow (Cook, Chan, et al., 2020), suggesting solute transport models and fluorescent tracers can be used as a proxy for microplastics within “real-world” settings for this flow regime. Given that microplastics should not be used for in situ tracer studies in freshwater systems, due to their hazardous impacts on the environment, it is important to understand how non-hazardous substances such as solute tracers can be used to represent the relevant transport mechanisms responsible for the transport and re-distribution of microplastics in fluvial environments. Cook, Chan, et al. (2020) focused only on the simple case of open channel flow and did not consider complex turbulence structures and small-scale eddies that occur across a vegetated channel with submerged canopy for both solutes and microplastics. Analyzing microplastic movement in response to these effects improves the existing hydrodynamic-based models and develops techniques that are much more applicable to real-world river systems.

Vegetation is ubiquitous in freshwater environments and alters the hydrodynamics of the system it is present within (Li & Zhang, 2010; Murphy et al., 2007; Shucksmith et al., 2011), making it a catalyst for altering the mixing processes of solutes. Within submerged vegetation, lower mean velocities are inside the vegetation canopy than that of the water column above (Lightbody & Nepf, 2006; Murphy et al., 2007; Nepf & Ghisalberti, 2008; Nepf, Sullivan, & Zavistoski, 1997) and flow paths become circuitous in motion as they bend around plant stems giving rise to variances in velocities (Nepf, Mugnier, & Zavistoski, 1997). These fluctuations in velocity generate distinct mixing regimes within the water column that vary over depth, and likely impact microplastic transport. Canopy height and density, along with river depth and discharge can vary depending on the season (Zhang et al., 2012) and climate change is expected to increase the frequency, intensity, and impacts of extreme weather events such as flooding and droughts (UK Centre for Ecology and Hydrology, 2021). With vegetation being more commonly used for flood protection (Dong et al., 2020; Geilen et al., 2004; Kourgialas & Karatzas, 2013; Salauddin et al., 2021; Vuik et al., 2016) and ever-present in fluvial systems, there is a significant need to quantify the impact of different canopy heights and densities on the transport and fate of microplastics. Recent research has documented the effects of microplastics on vegetation (De Souza Machado et al., 2019; Lehmann et al., 2020; Rillig et al., 2019) and the effects vegetation has on solute dispersion is well known (Li & Zhang, 2010; Lightbody & Nepf, 2006; Murphy et al., 2007; Nepf & Ghisalberti, 2008; Nepf, Mugnier, & Zavistoski, 1997; Shucksmith et al., 2011), but no research has been performed on the effects vegetation has on the transport of microplastics using fluorometric techniques or solute dispersion theory.

Fluorescent dyes such as Rhodamine WT have previously been used to trace concentrations of solutes within surface and groundwater studies (Chandler et al., 2016; Cook, Chan, et al., 2020; Cook, Price, et al., 2020; Harden et al., 2003; Nepf, Sullivan, & Zavistoski, 1997). If neutrally buoyant microplastics are shown to behave the same as fluorescent dyes under multiple flow regimes, then existing solute transport models can be applied to track

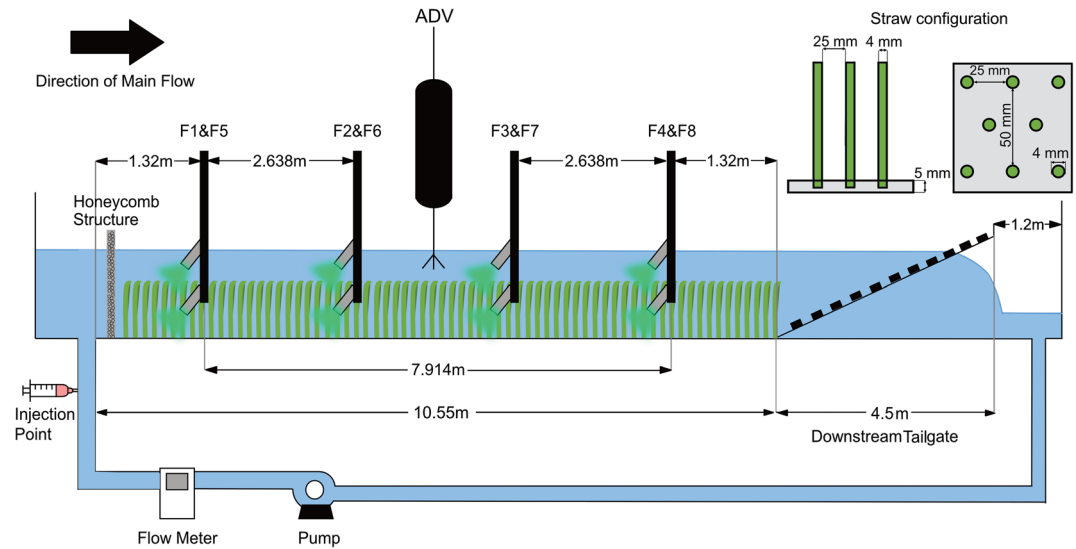


Figure 1. 2D Illustration of the experimental flume set-up (not to scale).

and trace microplastics within different aquatic environments, ultimately determining their fate. Calculating the longitudinal dispersion coefficient (LDC) is one such method (Chikwendu, 1986; Elder, 1958; Taylor, 1954) and can be achieved through a variety of techniques such as fluorometry, particle image velocimetry (PIV), and planar laser induced fluorescence (PLIF). Fluorometers can track fluorescent signatures, by detecting and quantifying them in real-time in both laboratory and field settings with relative ease and have previously been used for microplastics by Abolfathi et al. (2020), Boos et al. (2021), and Cook, Chan, et al. (2020). However, PIV and PLIF measurements require the use of lasers and shore-based cameras, causing them to be primarily implemented in laboratory-based studies over short timescales (Daigle et al., 2013).

Cook, Chan, et al. (2020) developed a method for chemically tagging microplastics with Nile red dye (excitation/emission: 552/636 nm), which gives off a fluorescent signature similar to that of Rhodamine (excitation/emission: 555/580 nm), enabling them to be accurately traced in a laboratory or field setting using fluorometers in real-time in the same experimental setup (Figure 1). Due to the difficulty obtaining pre-stained microplastic polymers of specific sizes, Cook, Chan, et al.'s (2020) microplastic staining technique was adopted to widen fluorometric applicability regarding microplastics and specifically trace PE's behavior over submerged canopies with the aim of improving current understanding of the physical mechanisms that govern microplastic mixing and dispersion within these complex flows. The physical effects of vegetation were simulated in a laboratory flume using flexible straws, following previously proven methodological approaches (e.g., Li & Zhang, 2010; Murphy et al., 2007; Nepf, Mugnier, & Zavistoski, 1997; Nepf & Ghisalberti, 2008; Nepf, Sullivan, & Zavistoski, 1997), and the effects of vegetation submergence depth on the transport behavior of microplastics were quantified. The majority of studies have utilized sediment transport techniques to analyze microplastic movement (Waldschläger et al., 2022), while limited data is available to validate the hypothesis of neutrally buoyant microplastics following similar transport pathways to that of solutes. LDC's for spherical neutrally buoyant PE were determined and compared with those measured from Rhodamine WT dye along with analytical solutions for the advection-dispersion equation to propose a mixing model for neutrally buoyant microplastics of a similar density to water. Existing well-established dispersion models are predominantly derived and validated for plain open channel flows and do not provide insight into mixing within vegetated flows. This paper, for the first time, identified and quantified the underlying mixing mechanisms of microplastics for complex flows over a submerged canopy.

2. Material and Methods

2.1. Experimental Setup

*PE (434,272, Sigma-Aldrich) of 40–46 μm in diameter was used due to it being one of the most common plastic polymers found in rivers across the globe (Horton et al., 2017; Rowley et al., 2020; van Emmerik &

Schwarz, 2019). The PE used in this study is spherical and represents a class of microplastics which are neutrally buoyant and therefore can be modeled using solute transport techniques. The PE was stained with Nile red dye (technical grade, N3013, Sigma-Aldrich) and Rhodamine WT dye was employed as the fluorescent solute to be used as a comparison for the dispersion of PE. Longitudinal dispersion measurements were conducted in a 0.34 m wide, 20 m long recirculating rectangular flume (Figure 1) made from glass reinforced plastic with a depth ranging from 0.248 to 0.254 m due to the variability at higher discharges and differing vegetation conditions. The wave dissipating weir was 4.5 m long (depending on angle) and acted as a downstream tailgate that could be altered to maintain the flow depth of 0.25 m. Velocities for the concentration data were calculated relative to the position of the top fluorometers through Equation 1 and highlighted in Figure 1 as F1, F2, F3, and F4.

$$u = \frac{x_4 - x_1}{\mu_4 - \mu_1}, \quad (1)$$

where x_4 and x_1 represent the distance from the inlet (the location of the fourth and first fluorometers) and μ_4 and μ_1 is the travel time between the centroids (s) of the fourth and first fluorometers respectively. The top fluorometers were selected for the main LDC results due to the excitation and emission of light covering a larger proportion of the water column, especially within the mixing and free flow zones (see Section 2.5). Bottom fluorometers were used for supplementary data and labeled F5, F6, F7, and F8. Turner Designs cyclops-7 fluorometers originally calibrated for Rhodamine WT's signature were used in the experiments. Velocity data for the *N*-zone model was collected using an Acoustic Doppler Velocimeter (ADV) positioned near the center of the flow length section to accurately record 3D water velocity measurements.

Concentration data was gathered through fluorometers positioned 2.6 m apart at 30 deg angles, ensuring maximum detection of the tracer cloud in the center of the flow and encompassing its distribution at depth. The fluorometers used Rhodamine WT optics with a linear range of 0–1000 ppb and a minimum detection limit of 0.01 ppb so that both Rhodamine dye and Nile red stained PE could be traced. To test the quality of data measurements recorded by the fluorometers, linear calibrations were performed in which a minimum R^2 value > 0.99 was obtained and used to convert voltages to ppb and mg/l for both dye and PE (Figures S1a and S1b in Supporting Information S1). Calibrations were performed in a 5-L beaker with a Hei-TORQUE Core overhead stirrer to enable the PE to be well-mixed and not float when no turbulence or advection is present. Calibrations for PE indicated a slightly wider spread in the voltages recorded by the fluorometers, although all show a linear relationship with a R^2 value > 0.99 (Figures S1a and S1b in Supporting Information S1). Fluorometers used a $\times 10$ gain, logged at a rate of 10 Hz, and are illustrated by gray rectangles emitting a green light in the experimental setup (Figure 1). Nepf, Sullivan, and Zavistoski (1997) showed that both velocity and turbulence intensity measured within cylindrical plastic model vegetation mimics profiles measured within real vegetation in both field and laboratory flows when compared to other studies. Therefore, plastic straws were glued into circular divots made in the simulated channel bed (made of PVC sheets) designed to imitate a uniform dense vegetation canopy made up of stems and removed for the base condition of open-channel flow. These are highlighted in green in Figures 1 and 2. It is important to consider that when present, submerged leaves in natural vegetation increase drag and diminish velocities when compared to regions occupied by stems and may affect the outcome of field experiments.

2.2. Experimental Processes

Three experimental scenarios were designed for this study including one scenario with no vegetation (NV), and two scenarios with a canopy of varying stem heights. Vegetation lengths of 0.1 m for low vegetation (LV), and 0.2 m for high vegetation (HV) were chosen (Figure 2) and removed for the base condition of open-channel flow (NV). The LV and HV flow regimes contained $\frac{H}{h_1}$ values of 2.5 and 1.25 in that order, where H is the channel depth (m) and h_1 is the height of the vegetation canopy. Each straw had a diameter of 4 mm and was placed in equally spaced rectangles 25 mm from the straw in front of it (parallel to the flow direction) and 50 mm from the straw to beside it. Subsequently, a fifth straw was inserted in the middle of each rectangle. Three replicates were used for both Rhodamine and PE injections for four different initial discharges of 0.005, 0.009, 0.013, and 0.017 m³/s at the inlet pipe in accordance with both Cook, Chan, et al. (2020) and Guymer and Environment Agency, 2002 to approximate discharges experienced by UK rivers. These were logged for 6, 5, 4, and 3 min respectively within each of the different canopy heights. Logging started and stopped at least 30 s before and

Fig. 2a

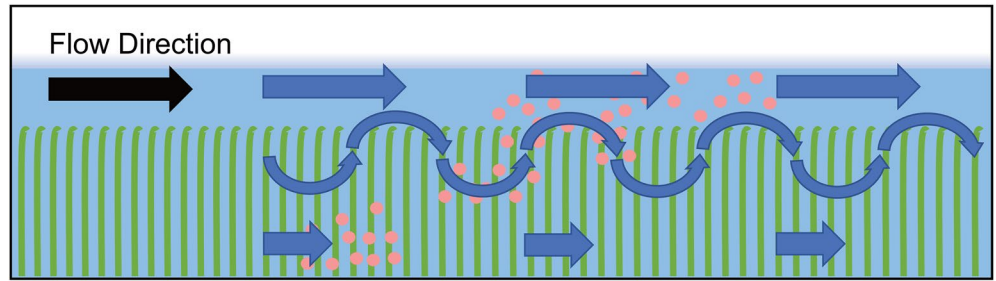


Fig. 2b

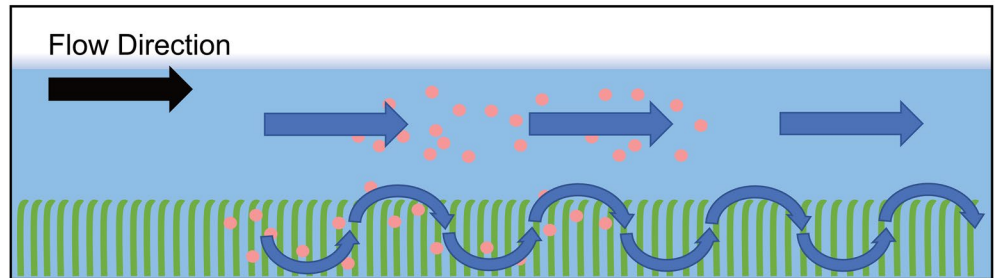


Figure 2. Visual illustration of the flow physics within (a) high (0.2 m) and (b) low (0.1 m) canopy heights in relation to a constant depth (0.25 m).

after fluorescence was injected/detected. Injections were made before the flow inlet from the pump which was located before the first straws within the flume (Figure 1). 10 ml of Rhodamine WT at 3000 ppb and 1.5 g of Nile red stained PE with <10 ml of water was well-mixed into a syringe before each injection. Table 1 provides a summary of these different conditions. Reynolds numbers for each velocity were calculated through Equation 2 (Nepf, 2004):

$$Re = \frac{uH}{\nu}, \quad (2)$$

where u is the velocity (m/s) and ν is the kinematic viscosity (m^2/s).

Velocity data can only be retrieved at least 40 mm away from the end of the ADV transmitter, requiring predictions to be made for the top 40–50 mm of the water column. Correlations and velocities were averaged from all four beams produced by the ADV to ensure quality data. If velocity measurements had correlation values below 0.8, they were highlighted and removed. Spikes in the ADV data were highlighted using a threshold calculated from the surrounding datapoints and replaced using a smoothed estimate outlined in Goring and Nikora (2002). Sampling for velocity measurements occurred at a rate of 100 Hz for a 5 min duration for each 32 mm range over the 250 mm water depth in the flume for each flow condition. For the vegetative conditions, fitted velocity measurements were interpolated using a polynomial function in order to produce uniformly distributed velocity profiles over the water column. Open channel flow velocities were theoretically predicted using logarithmic law through rearranging Equation 3:

$$u_* = \frac{uk}{LN\left(\frac{H}{y_0}\right)}, \quad (3)$$

where u_* represents shear velocity from the bottom of the channel (m/s), k is the Von Karman constant, H is the mean channel depth (m), and y_0 is the relative roughness of the channel bed (depending on the material) divided by 30 for hydraulically rough flows.

With the flow inlet from the pump in Figure 1 being perpendicular to the direction of the flow a honeycomb structure was implemented to straighten the flow (Figure 1) after a visible bifurcation effect originally caused $\frac{D_x}{Hu_*}$ to be lower for the base condition of open channel flow, where D_x is the longitudinal dispersion coefficient in

Table 1
Summary of Experimental Flow Conditions and Parameters

n	Initial Q (m³/s)	Depth-averaged velocity (m/s)	Average canopy velocity (m/s)	Average free flow velocity (m/s)	Flow depth (m)	Canopy height (m)	Stem diameter (m)	Reynolds number (Re)	u _s	u _{shc}	Longitudinal dispersion coefficient (m²/s)		
											Measured dye	Measured PE	N-zone
3	0.005	0.060	N/A	N/A	0.25	0	0.004	14,245	0.0031	N/A	0.0037	0.0031	0.0046
3	0.005	0.047	0.022	0.064	0.25	0.1	0.004	11,124	0.0024	0.0384	0.0148	0.0112	0.0094
3	0.005	0.053	0.040	0.093	0.25	0.2	0.004	12,686	0.0027	0.0221	0.0191	0.0166	0.0226
3	0.009	0.108	N/A	N/A	0.25	0	0.004	25,777	0.0056	N/A	0.0075	0.0085	0.0083
3	0.009	0.083	0.037	0.114	0.25	0.1	0.004	19,675	0.0043	0.0384	0.0222	0.0156	0.0202
3	0.009	0.102	0.077	0.183	0.25	0.2	0.004	24,130	0.0052	0.0221	0.0327	0.0329	0.0449
3	0.013	0.155	N/A	N/A	0.25	0	0.004	36,858	0.0079	N/A	0.0118	0.0110	0.0119
3	0.013	0.120	0.063	0.158	0.25	0.1	0.004	28,585	0.0062	0.0384	0.0312	0.0341	0.0288
3	0.013	0.136	0.107	0.229	0.25	0.2	0.004	32,159	0.0070	0.0221	0.0503	0.0451	0.0510
3	0.017	0.208	N/A	N/A	0.25	0	0.004	49,524	0.0107	N/A	0.0139	0.0140	0.0159
3	0.017	0.154	0.079	0.204	0.25	0.1	0.004	36,580	0.0079	0.0384	0.0466	0.0487	0.0498
3	0.017	0.159	0.127	0.263	0.25	0.2	0.004	37,579	0.0081	0.0221	0.0655	0.0707	0.0570

Note. Where n is the number of replicates, Q is the initial discharge in the pipe, u_s is the bed shear velocity, and u_{shc} is the shear velocity at the top of the vegetation canopy.

m²/s. Bifurcation is particularly rare within real-world settings and therefore not applicable to this study, however within open channel flow the initial tests resulted in the flow physics producing a low $\frac{D_x}{Hu_s}$ when measured against the concentration data. Based on these results, bifurcation causes lower LDC's when employing fluorometric techniques. This is potentially due to the bulk of both the dye and PE concentrations snaking around certain fluorometers instead of flowing through the optical sensors. More research is needed on the effect bifurcation has on longitudinal dispersion inside open channels, but it is outside the scope of this study. For future studies, when using flumes that have pipes perpendicular to the channel (Figure 1), implementing a honeycomb structure to straighten the flow is recommended.

2.3. Longitudinal Dispersion

Taylor's (1954) fundamental analysis is widely recognized as a proven technique for calculating the longitudinal dispersion of a solute within turbulent flow. Taylor (1954) found that after an adequate amount of time, a solute being injected into a cross-sectional area containing a solvent exhibiting uniform flow conditions will form a Gaussian distribution along the longitudinal axis. Using a Fickian diffusion-type expression within the one-dimensional advection-dispersion equation (ADE) this effect is shown in Equation 4

$$\frac{\partial c}{\partial t} + u \frac{\partial c}{\partial x} = D_x \frac{\partial^2 c}{\partial x^2}, \tag{4}$$

D_x is hydrodynamical dispersion considering the effects of advection, molecular diffusion, and shear dispersion, c represents the cross-sectional mean concentration (kg/m³), t is time (s), x is distance (m). LDC's were generated from the temporal concentration distribution of each tracer injection. Background removal was implemented by subtracting the mean of the last 25 s of data collection for each concentration curve. Cutoff values for the start and end of the peaks were selected using approximately 5% of the peak concentration and were checked by plotting the values on the respective distributions. Smoothing was implemented through a running average containing 1% of the total number of data points, enabling a larger or smaller window to be implemented depending on the logging length/discharge. Moments of the distributions were calculated (Rutherford, 1994) and a regression was fitted to calculate the gradient of time to centroid against the variance. LDC's were then established through Equation 5 (Fischer, 1966) and confidence intervals of LDC's were determined by first calculating the standard deviation (σ²) and applying an α value of 5%.

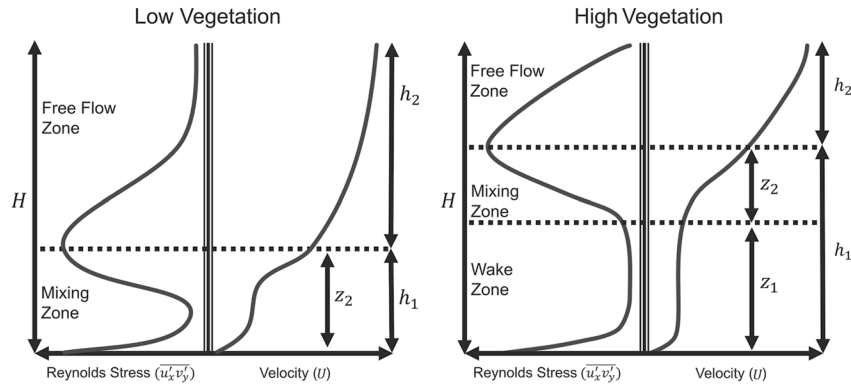


Figure 3. Conceptual model illustrating the relationship over a vertical profile between primary velocity and Reynolds stress through low and high submerged vegetation.

$$D_x = \frac{1}{2} u^2 \frac{d\sigma_t^2}{dt}, \quad (5)$$

where (σ_t^2) is the standard deviation of the response curves.

Given an idealized vertical velocity profile, Elder (1958) derived an equation that can theoretically predict D_x by accounting for the effects of shear dispersion through Equation 6

$$D_x = 5.93 H u_*^2, \quad (6)$$

Rutherford (1994) showed that u_* can be calculated through simply dividing the depth-averaged velocity u by anywhere between 10 and 20 depending on the roughness of the riverbed. This method was used as a reference for calculating u_* and applying logarithmic law in open channels through Equation 3. Elder's (1958) equation is widely used due to its simplicity and that it is based on fundamental mechanisms that are widely accepted. However, Elder's (1958) equation assumes a logarithmic velocity profile across the depth of the channel and does not account for potential fluctuations in velocity. Chikwendu (1986) developed an N -zone model that divides the channel cross-section into an infinite number of zones (j) in agreement with Taylor's (1954) original formulas. Mixing in each zone is dependent on the velocity differences of the zones either side of it $(q_1 + q_2 + \dots + q_j)^2 [1 - (q_1 + q_2 + \dots + q_j)]^2 [u_{1,2,\dots,j} - u_{(j+1),\dots,N}]^2$ divided by the vertical diffusivity $b_{j(j+1)}$ with the longitudinal diffusivity $\sum_{j=1}^N q_j D_{xj}$ added to the total

$$D_x(N) = \sum_{j=1}^{N-1} \frac{(q_1 + q_2 + \dots + q_j)^2 [1 - (q_1 + q_2 + \dots + q_j)]^2 [u_{1,2,\dots,j} - u_{(j+1),\dots,N}]^2}{b_{j(j+1)}} + \sum_{j=1}^N q_j D_{xj}, \quad (7)$$

where $j = (1, 2, \dots, N)$, $q = \frac{h_j}{H}$, D_{xj} is the average longitudinal diffusivity, and h_j is the thickness of each zone. The average vertical diffusivity between each zone is calculated by

$$b_{j(j+1)} = \frac{2D_{zj(j+1)}}{H^2(q_j + q_{j+1})}, \quad (8)$$

where $D_{zj(j+1)} = H k u_* q(1 - q)$ using Elder's (1958) equation for vertical diffusivity or $D_{zj(j+1)} = \frac{k u_* H}{6}$ when using a depth-averaged value (Jobson & Sayre, 1970).

2.4. Longitudinal Dispersion in Vegetated Flows

Vegetation makes the hydrology within river systems more complex and harder to model and/or predict the transport and fate of the pollutant in question. Reynolds stress and velocities vary over depth (Figure 3); therefore, a logarithmic velocity profile cannot be assumed when submerged vegetation is present. Longitudinal dispersion is consequently split into zones of mixing that vary over the vertical in size and number depending on the vegetation

conditions present. These can include a wake zone, a mixing zone, and a free flow zone which are illustrated in Figure 3. Using Chikwendu's (1986) model, Shucksmith et al. (2011) calculated $D_{z_j(j+1)}$ by considering both the velocity and shear stress profiles to represent the vertical diffusivity within the system more accurately in Equation 9. Vertical shear stress can be approximated through Reynolds stress in the mixing zone, assuming a Schmidt number of 1, defined as the net transfer of momentum across a surface within a turbulent fluid because of fluctuations in velocity.

$$D_{z_j(j+1)} = \frac{\tau_j}{\rho \frac{du}{dz_j}}, \quad (9)$$

ρ is the density of the fluid (kg/m^3) and τ_j is the Reynolds stress in each zone j (N/m^2). Within the wake zone a uniform velocity will occur because of low velocity gradients causing $\frac{du}{dz}$ to be near zero and Equation 9 to become redundant as limited mixing will take place due to shear. Mixing within the wake zone is expected to be mainly through diffusivity and Lightbody and Nepf's (2006) emergent salt marsh canopy equation can be used to calculate $D_x(N)$

$$D_x(N) = 0.17uS_d, \quad (10)$$

where u is the depth-averaged velocity in the wake zone (m^2/s). Above dense vegetation canopies the velocity profile can become logarithmic again in the free flow zone and the top of the canopy acts as another boundary layer requiring a need to estimate an equivalent shear velocity (Murphy et al., 2007; Shucksmith et al., 2011).

$$u_{*hc} = \sqrt{gh_2S_0}, \quad (11)$$

where g is acceleration due to gravity (m^2/s), h_2 is the height of free flow zone, and S_0 represents the bed slope. Therefore, using u_{*hc} mean vertical diffusivity $D_{z_j(j+1)}$ in the free flow zone can be calculated as

$$D_{z_j(j+1)} = \frac{Hku_{*hc}}{6}. \quad (12)$$

Accurately identifying the size of each zone is therefore very important to implementing the N-zone model correctly, leading to Nepf et al.'s (2007) equation which predicts mixing zone penetration depth:

$$\frac{z_2}{h_1} = \frac{CSL}{C_d N_v S_d h_1}, \quad (13)$$

where CSL is the canopy shear layer parameter with an empirical value of 0.23 ± 0.06 (Nepf et al., 2007), C_d is the vegetation drag coefficient, N_v is the vegetation density, and S_d is the stem diameter. Although this is a good reference for mixing zone penetration depth, Shucksmith et al. (2011) demonstrated it can be more accurately interpreted from Reynolds stress. Here, the N-zone model utilizes the peak Reynolds stress value to define the top of the mixing zone for Equations 9, 10, and 12 to be implemented correctly, which is visualized through Equation 9 in Figure S2 in Supporting Information S1.

3. Results

3.1. Concentration Data

Response curves from the different vegetated conditions conform to Gaussian distributions and are shown in Figure 4. An estimation of PE mass recovery between response curves indicated that $\geq 87\%$ advected straight through across all conditions between F1 and F4. As expected, the highest recovery percentage happened within open channel flow ($\geq 99\%$) and the lowest within LV ($\geq 87\%$) that mainly occurred at the slower initial discharges of 0.005 and 0.009 m^3/s . LDC's are displayed on the right-hand side of Table 1 and range from 0.0031 ± 0.0006 to 0.0140 ± 0.0016 m^2/s for both dye and PE within open channel flow for discharges ranging from 0.005 to 0.017 m^3/s . LDC's sorted by canopy height and including confidence intervals can be seen in Table S1 in Supporting Information S1. A few LDC's for the vegetative conditions overlapped on Figure 5 but generally dispersion increased with canopy height (h_1) compared to overall depth (0.25 m) and velocity. LV ($\frac{H}{h_1} = 2.5$) LDC's ranged from 0.0115 ± 0.0039 to 0.0487 ± 0.0042 m^2/s and HV ($\frac{H}{h_1} = 1.25$) LDC's ranged from 0.0166 ± 0.0017 to 0.0707 ± 0.0060 m^2/s , both in line with Shucksmith et al.'s (2011) cropped vegetation and

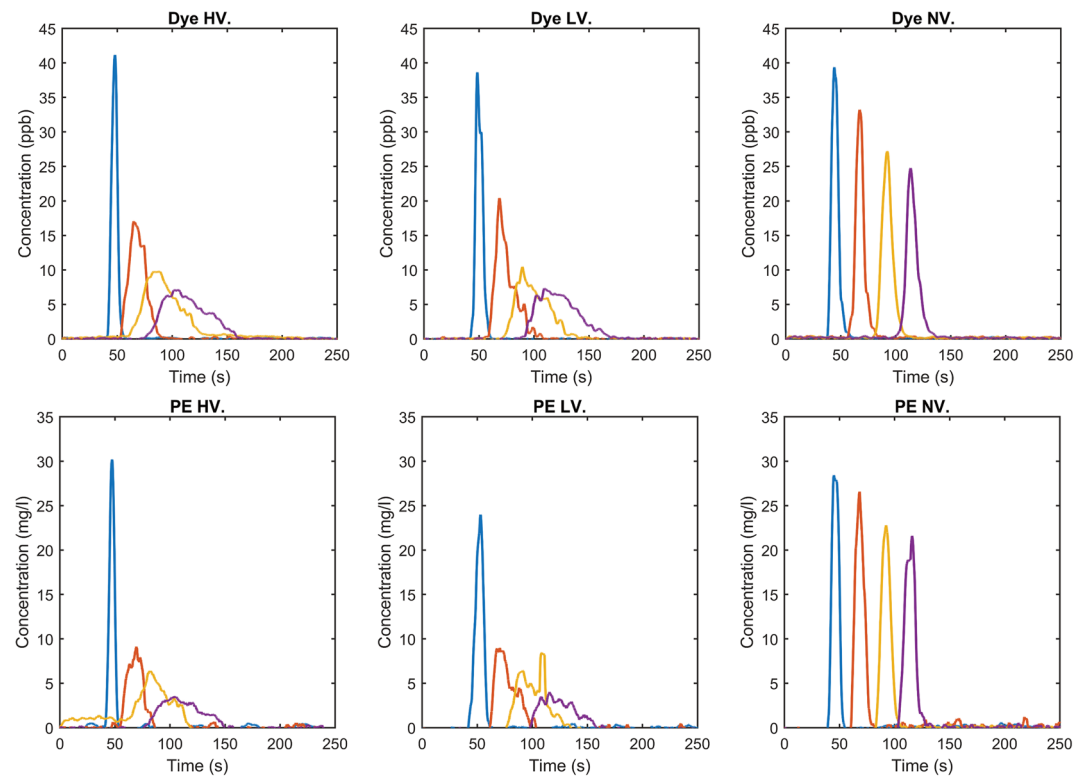


Figure 4. Response curves of instantaneous injections for dye (Rhodamine) and microplastic particles (PE) plotted as concentration (ppb for dye and mg/l for PE) against time (s) within HV, LV, and NV flow regimes at a discharge of $0.009 \text{ m}^3/\text{s}$.

Murphy et al.'s (2007) model canopy values. R^2 values > 0.95 for LDC's against velocity were achieved for every condition (Figure 5). Using Equation 1), velocities for both dye and PE were comparative to each other across all flow regimes ranging from $0.05827 \pm 0.0002 \text{ m/s}$ for the flow rate of 5 l/s to $0.209215 \pm 0.0005 \text{ m/s}$ for 20 l/s .

3.2. N-Zone Model

LDC's for both dye and PE were compared to Chikwendu's (1986) *N*-zone model across all test conditions. For NV, the *N*-zone model achieved a factor ($\frac{D_x}{Hu_*}$) of 5.93 in line with Elder's (1958) equation when using both an idealized velocity profile from the channel bed and a $\frac{u}{u_*}$ of 19.3. The *N*-zone model provided analogous results to the mean LDC's for both dye and PE shown in Figure 5. The $\frac{D_x}{Hu_*}$ values for LV and HV of 15.6 and 34.3 reinforce existing theory suggesting submerged vegetation velocity profiles differ from a logarithmic boundary layer due to the creation of a semipermeable boundary layer generated through drag created at the top of the canopy (Ghisalberti & Nepf, 2005). Fitted and measured velocity profiles collected from the ADV can be seen below for the differing initial discharges in Figure 6. Using Shucksmith's (2011) adaptation of Chikwendu's (1986) *N*-zone model, accurate LDC's were predicted for the LV and HV conditions. LDC's appeared to show more variability for the HV condition (Figure 5) and at higher velocities, which is expected due to increased turbulence and resultingly higher noise level produced by fluorometers being positioned closer to the canopy. Rhodamine dye and PE demonstrated analogous relationships with the *N*-zone model through root mean square values (RMSE) and percent differences (Table 2). Overall, *N*-zone predicted LDC's were within 10% for every experimental condition, specifically within 9.32% accuracy for dye, and 9.83% accuracy for PE under the NV, LV, and HV regimes (Table 2).

3.3. Microplastics Versus Dye

The LDC regressions and both the percentage difference and RMSE analysis indicate that PE dispersed equally to dye across all flow regimes. The largest percentage differences happened between PE and dye and the *N*-zone

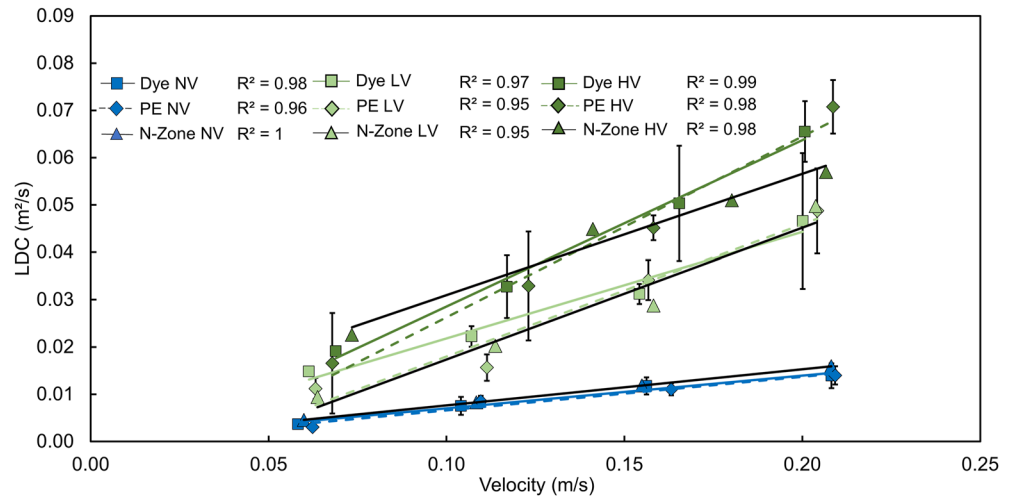


Figure 5. Mean LDC correlations for dye, PE, and theoretical *N*-zone values ($\pm 95\%$ confidence intervals) versus velocity for the different vegetated conditions (NV, LV, HV).

model within the slowest discharges of 0.005 and 0.009 m³/s across all the conditions. This was potentially due to the dispersion coefficients being low themselves, exaggerating the differences (Table S1 in Supporting Information S1) or minor differences between PE and dye dispersion due to PE being slightly less than neutrally buoyant and advection playing a less dominant role at lower discharges. Further analysis between the raw LDC data for dye and PE within the slowest discharges revealed no significant difference between the two populations (Welch's *t*-test $p > 0.05$). For six of the eight flow rates within the vegetated conditions (Table S1 in Supporting Information S1), dye and PE percent differences were dispersing within a 15.06% range of each other and within 6.12% for each vegetated condition (Table 2). This was supported through the regression containing an R^2 value of 0.98 and a gradient of 1.06 \times when dye and PE were plotted against each other (Figure 7). The RMSE analysis displayed slightly better values using dye as the predicted value for PE dispersion than the *N*-zone model, indicating that dye is an agreeable substitute when used as a proxy for neutrally buoyant microplastic movement. As expected, LDC's and variability (95% confidence intervals) increased with higher velocities as shown by the regression and longer error bars in Figure 7.

4. Discussion

4.1. Applicability of Microplastic Tracing and Hydrodynamic Modeling

Fluorometers calibrated for Rhodamine emission and excitation wavelengths of 555 and 580 nm were found to accurately predict neutrally buoyant microplastic dispersion in complex flow regimes, widening their current proven applicability from open channels to additional flow environments. The microplastic staining technique is applicable for field use but microplastic concentrations in nature may be lower than within laboratory flumes and microplastic fluorescence will degrade over time when subjected to natural light, making it less applicable to studies running over large timescales. Therefore, the *N*-zone model, with the additional equations to account for different mixing zones over depth, is shown to be capable of approximating the amount of mixing if you know the velocity structure of the river in question. In addition, an ethically sound and easily available solute tracer such as Rhodamine WT can be used in the field as a proxy for neutrally buoyant microplastics of a specific size range (see Section 4.3) over short timescales within complex flows in the water column based on the findings presented here. The advection-dispersion equation used to calculate dispersion coefficients is not influenced by high or low concentrations due it being deterministic as long as the areas under the separate response curves are from the same instantaneous injection and are readable by the fluorometers when compared to background concentrations. The same techniques used in this study can be applied to lower canopy densities where a similar outcome is anticipated to the LV condition where vortices penetrate to the bed and dominate the mixing processes in both cases (Murphy et al., 2007; Poggi et al., 2004; Shucksmith et al., 2011). These techniques can also be employed on living vegetation as proved by Shucksmith et al. (2011) utilizing submerged *Carex* plants

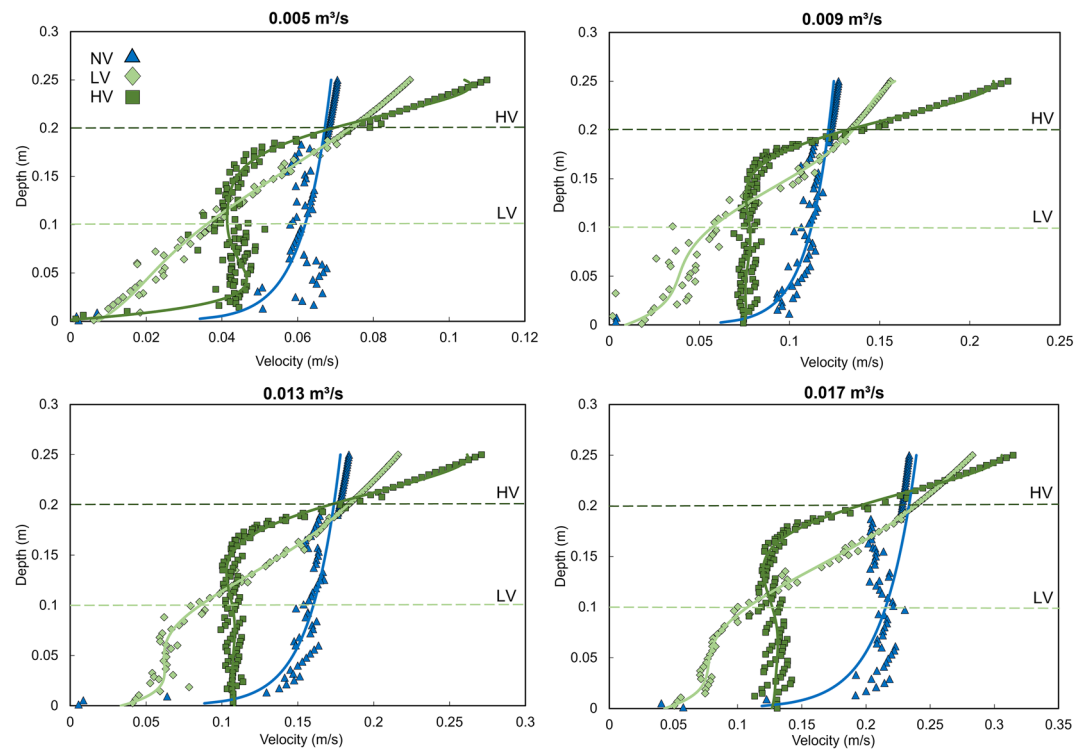


Figure 6. Fitted and measured velocity profiles for 0.005, 0.009, 0.013, 0.017 m³/s discharges within the NV, LV, and HV conditions.

in their study. Aggregation between PE and the model vegetation and walls of the flume did take place but not a significant amount as indicated by the mass recovery from the response curves. Given the differing surface properties of the straws and natural vegetation we would predict that the lack of aggregation presented here would be indicative of those with woody stems. Microplastic type and shape likely has a larger influence on aggregation (Wang et al., 2021) than the difference between natural vegetation and straws which is outside the scope of the study. More research is required on microplastic aggregation with living vegetation before any conclusions are made. It is worth noting we observed a visible “wall creeping” effect for a small percentage of the microplastics as seen in Eitzen et al. (2019) study. PE particles would attach themselves to the glass walls of the flume through adsorption, but this was not a significant amount when compared to the bulk tracer cloud that advected straight through, demonstrated in Figure 4.

Since PE is a solid particle and not a solute, the response curves generate more scattered dispersion bands, causing the voltage readings to vary slightly as the particles pass through the optical sensor. This does not affect the calculated dispersion after smoothing, as demonstrated in Cook, Chan, et al. (2020), and we would expect the same phenomenon to occur for other stained solid particles used for fluorometric tracing. In theory, fluorometric techniques can be utilized to trace stained solid particles of a near neutral buoyancy

Table 2
LDC Root Mean Square Error (RMSE) Comparison Between Dye, PE, and the N-Zone Model for the Different Vegetated Conditions

Vegetation Condition	% Difference PE versus Dye	% Difference Dye versus N-zone	% Difference PE versus N-zone	RMSE		
				PE versus Dye	Dye versus N-zone	PE versus N-zone
NV	0.56	9.32	9.83	0.00069	0.00117	0.00130
LV	4.49	6.12	1.36	0.00417	0.00350	0.00366
HV	1.42	5.56	5.76	0.00391	0.00763	0.01006

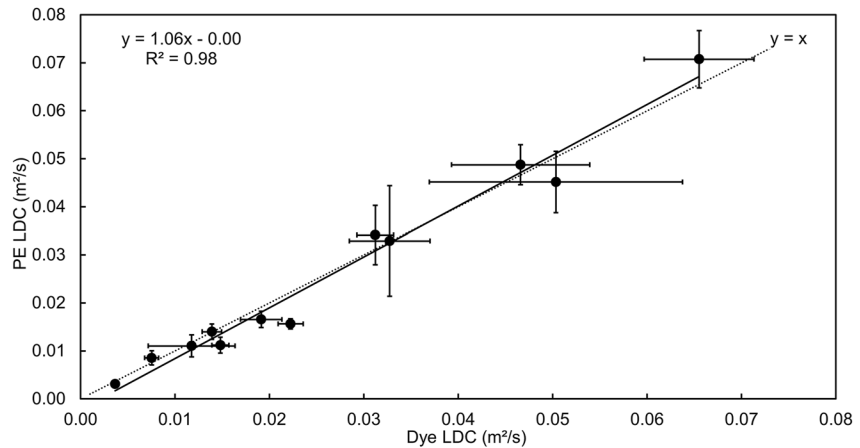


Figure 7. Mean PE LDC's versus mean dye LDC's for all conditions ($\pm 95\%$ confidence intervals).

displaying the correct wavelengths for the employed instruments. Boos et al. (2021) demonstrated that fluorometric quantification for microplastics in fluvial environments worked best for smaller microplastic sizes of 1 μm . Our study builds on this demonstrating that fluorometric techniques can be used for microplastic particles up to 46 μm . More research is needed to investigate the upper size limit of solid particle movement where the signal fluctuation through the optical sensor is too high to accurately quantify. This demonstrates ample opportunity within future research to calculate the dispersion of any pollutant that meets these criteria. As a result, the applicability of fluorometric tracing can be significantly widened beyond solutes. The N-zone model predicted LDC's to within 5.76% across the vegetated conditions (Table 2), thus analyzing velocities over depth can be used to reasonably predict the dispersion of spherical neutrally buoyant PE over short timescales in fluvial environments. It is then a logical assumption that other hydrodynamic models that use velocity profiles may also provide insights into microplastic dispersion and may be used to quantify their mixing given the right conditions. It is important to understand these techniques quantify the physical mechanisms behind microplastic and solute transport and not the biological and chemical which is outside the scope of the study.

4.2. Flow Characteristics

The flow physics for both the LV and HV conditions are visualized in Figure 2 and modeled in Figure 3. The LV profiles are dominated by vortex driven exchanges that penetrate deep into the canopy where they reach the riverbed and are shot back out into the free flow zone. This causes the entire canopy to become a singular mixing zone, thus eliminating the wake zone (Figure 3). The LV condition displayed flow characteristics similar to Shucksmith et al.'s (2011) Carex plants at a height of 0.055 m, despite Shucksmith implementing a changing overall depth relative to the canopy height and ours being constant at 0.25 m, due to vortices penetrating to the bed in both cases. The LV condition was also analogous to Murphy et al.'s (2007) sparse canopy setting indicating that within these flow environments, vortices dominate the mixing processes. Thus, vortices govern longitudinal dispersion in submerged vegetation if they penetrate to the bed, producing two zones of mixing. At the lowest discharge of 0.005 m^3/s , the velocity profile for LV in Figure 6 exhibits a noticeable linear trend over depth when compared to other discharges for this condition whilst also exhibiting the slowest depth-averaged velocity of 0.047 m/s. Indicating that below a certain velocity, the differences between the mixing and free flow region are not significant enough to cause the canopy to exhibit a constant velocity at any stage over depth compared to a slight drag displayed in the top half of the canopies for the faster discharges of 0.009, 0.013, and 0.017 m^3/s . This may have had a minor effect on microplastic retention due to the slightly lower mass recovery percentage and larger percent differences shown in Sections 3.1 and 3.3, reinforcing the theory that advection plays an important role in microplastic retention. Flow domains where advection plays a less dominant role such as ponds and wetlands may provide key insights into microplastic retention in freshwater environments. The HV profiles are split into three separate zones where vortices from the free flow zone dominate the dispersion and only reach so far into the vegetation canopy, enabling sepa-

rate mixing and wake zones to be established (Figure 3). The HV condition matched Shucksmith's (2011) other cropped cases where the mixing was split into three zones instead of two. Dispersion occurs mostly in the mixing and free flow zones with very little contributing within the canopy wake zone. Identification of mixing zone penetration depth to the top of the wake zone (z_1) when using the N -zone model is therefore essential to accurately depict the flow physics of the channel. Fitted Reynolds stress profiles from the ADV velocities were used over the depth to predict the size of each zone and determine whether a wake zone was indeed present.

Reynolds stress for the vegetative conditions differed due to its impact on both the velocity and concentration profiles. Reynolds stress peaked at the top of the canopy (h_1) and at the bed of the flume, indicating two boundary layers are present within vegetative flow (shown in Figure 3) in accordance with Murphy et al. (2007) and Shucksmith et al. (2011). Reynolds stress values for each condition were predicted using an approximation of turbulent eddies via Equation 9. As flow rates increased, the Reynolds stress also increased causing more extreme profiles over the depth at the top of the canopy. Reynolds stress values within the wake zone were often negative, once again producing the need to provide an accurate representation of the mixing zone penetration depth within the N -zone model and correctly implement Equation 10, eliminating these negative values. Highlighting how many zones are present within the system is consequently instrumental to performing the correct analysis within the N -zone model. When comparing the size of the mixing zone over depth to other studies such as Guo and Chen (2022), the top of the mixing zone is located near the top of the canopy when implementing the N -zone model, as shown through the fitted vertical diffusivity profiles utilizing Equation 9 (Figure S2 in Supporting Information S1) and does not include the receding profile from the peak. Guo and Chen's (2022) vertical dispersion and velocity profiles over depth in dense canopies are in agreement with ours despite them implementing a larger $\frac{H}{h_1}$ of 3.36, indicating that the same principles utilized by the N -zone model to calculate vertical dispersion in different zones by Equations 9, 10, and 12 are applicable regardless of $\frac{H}{h_1}$.

4.3. Solute and Microplastic Dispersion

LDC's for neutrally buoyant microplastics (i.e., PE) and solutes (i.e., Rhodamine dye) were significantly correlated within submerged model vegetation irrespective of the complexity of the flow regime (i.e., Reynolds number) in the water column. The complexity of the flow regime within the water column did not affect microplastic dispersion inversely to a conventional solute such as Rhodamine. It is therefore reasonable to expect that microplastics of a near neutral buoyancy behave in the same manner as solutes from the riverbed to the flow surface no matter how fast or complicated the flow regime may be. These findings highlight that most microplastics, with properties similar to those tested in this study, will eventually be deposited in the ocean and not retained within river catchments once they enter the water column of fluvial systems. Nizzetto et al.'s (2016) study inferred that microplastics with a diameter of <0.2 mm were not retained in river catchments regardless of their density and only 16%–38% of microplastics with a higher density than water were retained. Below a certain size other factors such as shape and density become less significant because the smaller the particle, the more the relation between the gravitational force and surface force is reduced, thus diminishing the total amount of force that can act on them. Hoellein et al. (2019) suggested that particle shapes can affect microplastic transport, but also stated that even after biofilm colonization, if the density of the microplastic was less than water it would float. Drummond et al. (2022) also approximated only 5% of microplastics were subject to long-term accumulation per km in rivers, all supporting our findings that the majority of neutrally buoyant microplastics follow the same transport pathways as solutes and are not retained in river catchments. Over long timescales however, this small percentage is subject to incremental change and will likely become significant given large enough quantities resulting in microplastics potentially accumulating in “dead zones” within rivers (Guymer & Environment Agency., 2002; Wallis et al., 1989). Though, when subjected to turbulent flows these adsorbed microplastics may saltate over longer durations (Ji et al., 2014) resulting in temporary reintroductions into the main flow within the water column and once again reaching the ocean given a long enough timescale.

We recognize that the results of this data are limited to spherical PE particles transported within the water column but ultimately contribute to the end goal of validating solute transport techniques to accurately predict neutrally buoyant microplastic dispersion. It is expected that biofouling, along with different microplastic types, sizes, shapes, and densities may affect the transport and fate of microplastics above a certain size (Besseling et al., 2017; Bucci et al., 2020; Hoellein et al., 2019; Kaiser et al., 2017; Nizzetto et al., 2016). If particles are

below this size, we would expect similar results for other plastic polymers regardless of their type or shape if they have a near neutral buoyancy such as PS. However, Boos et al.'s (2021) study suggested that PS particles, with a density of 1.05 g/cm³ and at the lower microplastic size range of 1–10 μm, were retained in sediments and immobilized in the hyporheic exchange zone indicating there may be a lower size boundary for particle entrapment and more research on microplastic movement within other flow domains is needed. Immobilization in sediments may transpire for a small percentage of neutrally buoyant microplastic concentrations but the bulk concentration mass will remain in the water column given these findings. Density and size may then be the most important factors for smaller microplastics but, as suggested by Nizzetto et al. (2016), even microplastics with higher densities may not be retained in rivers if they are below a certain diameter. This study, for the first time, proposes and validates a dispersion model suitable for neutrally buoyant microplastics within complex flows influenced by submerged canopies. These results can consequently contribute to implementing a new technique for identifying the transport and fate of microplastics within rivers worldwide. To provide a more comprehensive understanding of the underlying mechanisms affecting microplastic transport these variables (e.g., particle's type, size, shape, and density) need to be investigated over a variety of timescales and flow domains to identify and quantify these effects on the dispersion of microplastics.

5. Conclusion

The dispersion and mixing processes of PE microplastics over submerged canopies were investigated using novel fluorometric tracing and particle staining techniques for the first time within a laboratory setting. The analysis of fluorometric and hydrodynamic data showed that distinct mixing zones were created over the canopy, which were primarily influenced by canopy physical characteristics (i.e., stem height). Neutrally buoyant PE dispersed interchangeably with Rhodamine in the water column regardless of the complexity of the flow regime instigated by submerged model vegetation. The results of the fluorometric analysis showed that Rhodamine WT dye can be used as a proxy over short timescales for field tests with spherical microplastics of a near neutral buoyancy (i.e., PE) in free-surface flows containing vegetated environments. It was shown that analytical solutions for mixing coefficients, as a result of the advection-dispersion equation and hydrodynamic modeling using velocity profiles (the *N*-zone model), are capable of accurately approximating PE mixing and dispersion over a canopy for a range of environmental flows with varying Reynolds numbers. Consequently, the proposed analytical solutions and newly developed tracing and staining techniques for determining the transport and fate of neutrally buoyant microplastics can help develop effective management strategies to enhance water quality across a variety of turbulent flow domains in the future.

Conflict of Interest

The authors declare no conflicts of interest relevant to this study.

Data Availability Statement

All data and code used in the analysis is available at the online repository of the University of Warwick, WRAP: <https://wrap.warwick.ac.uk/174908>.

References

- Abolfathi, S., Cook, S., Yeganeh-Bakhtiari, A., Borzooei, S., & Pearson, J. (2020). Microplastics transport and mixing mechanisms in the near-shore region. *Coastal Engineering Proceedings*, 36(36v), 63. <https://doi.org/10.9753/icce.v36v.papers.63>
- Abolfathi, S., & Pearson, J. (2017). Application of smoothed particle hydrodynamics (SPH) in nearshore mixing: A comparison to laboratory data. *Coastal Engineering Proceedings*, 35, 16. <https://doi.org/10.9753/icce.v35.currents.16>
- Allen, S., Allen, D., Phoenix, V. R., Le Roux, G., Jimenez, P. D., Simonneau, A., et al. (2019). Atmospheric transport and deposition of microplastics in a remote mountain catchment. *Nature Geoscience*, 12(5), 339–344. <https://doi.org/10.1038/s41561-019-0335-5>
- Anderson, J. C., Park, B. J., & Palace, V. P. (2016). Microplastics in aquatic environments: Implications for Canadian ecosystems. *Environmental Pollution*, 218, 269A–280. <https://doi.org/10.1016/j.envpol.2016.06.074>
- Barnes, D. K. A., Galgani, F., Thompson, R. C., & Barlaz, M. (2009). Accumulation and fragmentation of plastic debris in global environments. *Philosophical Transactions of the Royal Society B: Biological Sciences*, 364(1526), 1985–1998. <https://doi.org/10.1098/rstb.2008.0205>
- Besseling, E., Quik, J. T. K., Sun, M., & Koelmans, A. A. (2017). Fate of nano- and microplastic in freshwater systems: A modeling study. *Environmental Pollution*, 220, 540–548. <https://doi.org/10.1016/j.envpol.2016.10.001>

Acknowledgments

Funding was provided by the Natural Environmental Research Council (NERC) and The Central England NERC Training Alliance (CENTA). We also acknowledge our Civil Engineering Technician Ian Bayliss for help in setting up the experiment. NERC grant NE/S007350/1 (243303, BS).

- Boos, J. P., Gilfedder, B. S., & Frei, S. (2021). Tracking microplastics across the streambed interface: Using laser-induced-fluorescence to quantitatively analyze microplastic transport in an experimental flume. *Water Resources Research*, 57(12), 1–10. <https://doi.org/10.1029/2021WR031064>
- Bråte, I. L., Halsband, C., Allan, I., & Thomas, K. V. (2014). Report made for the Norwegian environment Agency: Microplastics in marine environments: Occurrence, distribution and effects (Issue March 2015).
- Bucci, K., Tulio, M., & Rochman, C. M. (2020). What is known and unknown about the effects of plastic pollution: A meta-analysis and systematic review. *Ecological Applications*, 30(2), 1–16. <https://doi.org/10.1002/eap.2044>
- Chandler, I. D., Guymer, I., Pearson, J. M., & van Egmond, R. (2016). Vertical variation of mixing within porous sediment beds below turbulent flows. *Water Resources Research*, 52(5), 3493–3509. <https://doi.org/10.1002/2015WR018274>
- Chikwendu, S. C. (1986). Application of a slow-zone model to contaminant dispersion in laminar shear flows. *International Journal of Engineering Science*, 24(6), 1031–1044. [https://doi.org/10.1016/0020-7225\(86\)90034-0](https://doi.org/10.1016/0020-7225(86)90034-0)
- Cook, S., Chan, H. L., Abolfathi, S., Bending, G. D., Schäfer, H., & Pearson, J. M. (2020). Longitudinal dispersion of microplastics in aquatic flows using fluorometric techniques. *Water Research*, 170, 115337. <https://doi.org/10.1016/j.watres.2019.115337>
- Cook, S., Price, O., King, A., Finnegan, C., van Egmond, R., Schäfer, H., et al. (2020). Bedform characteristics and biofilm community development interact to modify hyporheic exchange. *Science of the Total Environment*, 749, 141397. <https://doi.org/10.1016/j.scitotenv.2020.141397>
- Daigle, A., Bérubé, F., Bergeron, N., & Matte, P. (2013). A methodology based on Particle image velocimetry for river ice velocity measurement. *Cold Regions Science and Technology*, 89, 36–47. <https://doi.org/10.1016/j.coldregions.2013.01.006>
- de Souza Machado, A. A., Lau, C. W., Kloas, W., Bergmann, J., Bachelier, J. B., Faltin, E., et al. (2019). Microplastics can change soil properties and affect plant performance. *Environmental Science and Technology*, 53(10), 6044–6052. <https://doi.org/10.1021/acs.est.9b01339>
- Dong, S., Abolfathi, S., Salaudin, M., Tan, Z. H., & Pearson, J. M. (2020). Enhancing climate resilience of vertical seawall with retrofitting - a physical modelling study. *Applied Ocean Research*, 103(Febuary), 102331. <https://doi.org/10.1016/j.apor.2020.102331>
- Dris, R., Imhof, H. K., Löder, M. G. J., Gasperi, J., Laforsch, C., & Tassin, B. (2018). Microplastic contamination in freshwater systems: Methodological challenges, occurrence and sources. In *Microplastic contamination in aquatic environments: An emerging matter of Environmental Urgency*. <https://doi.org/10.1016/B978-0-12-813747-5.00003-5>
- Drummond, J. D., Schneidewind, U., Li, A., Hoellein, T. J., Krause, S., & Packman, A. I. (2022). Microplastic accumulation in riverbed sediment via hyporheic exchange from headwaters to mainstems. *Science Advances*, 8(2). <https://doi.org/10.1126/sciadv.abi9305>
- Edo, C., González-Pleiter, M., Leganés, F., Fernández-Piñas, F., & Rosal, R. (2020). Fate of microplastics in wastewater treatment plants and their environmental dispersion with effluent and sludge. *Environmental Pollution*, 259, 113837. <https://doi.org/10.1016/j.envpol.2019.113837>
- Eitzen, L., Paul, S., Braun, U., Altmann, K., Jekel, M., & Ruhl, A. S. (2019). The challenge in preparing particle suspensions for aquatic microplastic research. *Environmental Research*, 168, 490–495. <https://doi.org/10.1016/j.envres.2018.09.008>
- Elder, J. W. (1958). The dispersion of marked fluid in turbulent shear flow. *Journal of Fluid Mechanics*, 5(4), 544–560. <https://doi.org/10.1017/S0022112059000374>
- Eriksen, M., Lebreton, L. C. M., Carson, H. S., Thiel, M., Moore, C. J., Borror, J. C., et al. (2014). Plastic pollution in the World's oceans: More than 5 trillion plastic pieces weighing over 250,000 tons afloat at sea. *PLoS One*, 9(12), 1–15. <https://doi.org/10.1371/journal.pone.0111913>
- Erni-cassola, G., Gibson, M. I., Thompson, R. C., & Christie-oleza, J. A. (2017). Lost, but found with Nile red: A novel method for detecting and quantifying small microplastics (1 mm to 20 µm) in environmental samples. *Environmental Science & Technology*, 51(23), 13641–13648. <https://doi.org/10.1021/acs.est.7b04512>
- Fischer, H. (1966). *Longitudinal dispersion in laboratory and natural streams. Technical Report*. Keck Laboratory of Hydraulic and Water Resources, California Institution of Technology.
- Frias, J. P. G. L., & Nash, R. (2019). Microplastics: Finding a consensus on the definition. *Marine Pollution Bulletin*, 138(September 2018), 145–147. <https://doi.org/10.1016/j.marpolbul.2018.11.022>
- Geilen, N., Jochems, H., Krebs, L., Muller, S., Pedroli, B., van der Sluis, T., et al. (2004). Integration of ecological aspects in flood protection strategies: Defining an ecological minimum. *River Research and Applications*, 20(3), 269–283. <https://doi.org/10.1002/rra.777>
- Ghisalberti, M., & Nepf, H. (2005). Mass transport in vegetated shear flows. *Environmental Fluid Mechanics*, 5(6), 527–551. <https://doi.org/10.1007/s10652-005-0419-1>
- Goring, D. G., & Nikora, V. I. (2002). Despiking acoustic Doppler velocimeter data. *Journal of Hydraulic Engineering*, 128(1), 117–126. [https://doi.org/10.1061/\(asce\)0733-9429\(2002\)128:1\(117\)](https://doi.org/10.1061/(asce)0733-9429(2002)128:1(117))
- Guo, J., & Chen, G. (2022). Solute dispersion from a continuous release source in a vegetated flow: An analytical study. *Water Resources Research*, 58(4), 1–20. <https://doi.org/10.1029/2021WR030255>
- Guymer, I., & Environment Agency. (2002). A national database of travel time, dispersion and methodologies for the protection of river abstractions.
- Harden, H. S., Chanton, J. P., Rose, J. B., John, D. E., & Hooks, M. E. (2003). Comparison of sulfur hexafluoride, fluorescein and rhodamine dyes and the bacteriophage PRD-1 in tracing subsurface flow. *Journal of Hydrology*, 277(1–2), 100–115. [https://doi.org/10.1016/S0022-1694\(03\)00074-X](https://doi.org/10.1016/S0022-1694(03)00074-X)
- Hoellein, T. J., Shogren, A. J., Tank, J. L., Risteca, P., & Kelly, J. J. (2019). Microplastic deposition velocity in streams follows patterns for naturally occurring allochthonous particles. *Scientific Reports*, 9(1), 1–11. <https://doi.org/10.1038/s41598-019-40126-3>
- Horton, A. A., Svendsen, C., Williams, R. J., Spurgeon, D. J., & Lahive, E. (2017). Large microplastic particles in sediments of tributaries of the River Thames, UK – Abundance, sources and methods for effective quantification. *Marine Pollution Bulletin*, 114(1), 218–226. <https://doi.org/10.1016/j.marpolbul.2016.09.004>
- Jamieson, A. J., Brooks, L. S. R., Reid, W. D. K., Piertney, S. B., Narayanaswamy, B. E., & Linley, T. D. (2019). Microplastics and synthetic particles ingested by deep-sea amphipods in six of the deepest marine ecosystems on Earth. *Royal Society Open Science*, 6(2), 1–11. <https://doi.org/10.1098/rsos.180667>
- Jenner, L. C., Rotchell, J. M., Bennett, R. T., Cowen, M., Tentzeris, V., & Sadofsky, L. R. (2022). Science of the Total Environment Detection of microplastics in human lung tissue using µ FTIR spectroscopy. *Science of the Total Environment*, 831(March), 154907. <https://doi.org/10.1016/j.scitotenv.2022.154907>
- Ji, C., Munjiza, A., Avital, E., Xu, D., & Williams, J. (2014). Saltation of particles in turbulent channel flow. *Physical Review E - Statistical, Nonlinear and Soft Matter Physics*, 89(5), 1–14. <https://doi.org/10.1103/PhysRevE.89.052202>
- Jimoh, M., & Abolfathi, S. (2022). Modelling pollution transport dynamics and mixing in square manhole overflows. *Journal of Water Process Engineering*, 45(August 2021), 102491. <https://doi.org/10.1016/j.jwpe.2021.102491>
- Jobson, H. E., & Sayre, W. W. (1970). Vertical transfer in open channel flow. *Journal of Hydraulic Engineering*, 96(3), 703–724. <https://doi.org/10.1061/jycej.0002374>

- Kaiser, D., Kowalski, N., & Waniek, J. J. (2017). Effects of biofouling on the sinking behavior of microplastics. *Environmental Research Letters*, 12(12), 124003. <https://doi.org/10.1088/1748-9326/aa8e8b>
- Klemeš, J. J., Fan, Y. V., Tan, R. R., & Jiang, P. (2020). Minimising the present and future plastic waste, energy and environmental footprints related to COVID-19. *Renewable and Sustainable Energy Reviews*, 127(April), 109883. <https://doi.org/10.1016/j.rser.2020.109883>
- Kourgialas, N. N., & Karatzas, G. P. (2013). A hydro-economic modelling framework for flood damage estimation and the role of riparian vegetation. *Hydrological Processes*, 27(4), 515–531. <https://doi.org/10.1002/hyp.9256>
- Lehmann, A., Leifheit, E. F., Feng, L., Bergmann, J., Wulf, A., & Rillig, M. C. (2020). Microplastic fiber and drought effects on plants and soil are only slightly modified by arbuscular mycorrhizal fungi. *Soil Ecology Letters*, 4(1), 32–44. <https://doi.org/10.1007/s42832-020-0060-4>
- Leslie, H. A., van Velzen, J. M. M., Brandsma, S. H., Vethaak, D., Garcia-Vallejo, J. J., & Lamoree, M. H. (2022). *Discovery and quantification of plastic particle pollution in human blood*. Environment International. <https://doi.org/10.1016/j.envint.2022.107199>
- Li, C. W., & Zhang, M. L. (2010). 3D modelling of hydrodynamics and mixing in a vegetation field under waves. *Computers & Fluids*, 39(4), 604–614. <https://doi.org/10.1016/j.compfluid.2009.10.010>
- Lightbody, A. F., & Nepf, H. M. (2006). Prediction of velocity profiles and longitudinal dispersion in emergent salt marsh vegetation. *Limnology & Oceanography*, 51(1), 218–228. <https://doi.org/10.4319/lo.2006.51.1.0218>
- Miller, M. E., Hamann, M., & Kroon, F. J. (2020). Bioaccumulation and biomagnification of microplastics in marine organisms: A review and meta-analysis of current data. *PLoS One*, 15(10), 1–25. <https://doi.org/10.1371/journal.pone.0240792>
- Murphy, E., Ghisalberti, M., & Nepf, H. (2007). Model and laboratory study of dispersion in flows with submerged vegetation. *Water Resources Research*, 43(5), 1–12. <https://doi.org/10.1029/2006WR005229>
- Nepf, H. M. (2004). Vegetated flow dynamics introduction: Scales of morphology and flow in a tidal marsh. *Coastal and Estuarine Studies*, 59, 137–163. <https://doi.org/10.1029/CE059p0137>
- Nepf, H. M., & Ghisalberti, M. (2008). Flow and transport in channels with submerged vegetation. *Acta Geophysica*, 56(3), 753–777. <https://doi.org/10.2478/s11600-008-0017-y>
- Nepf, H. M., Ghisalberti, M., White, B., & Murphy, E. (2007). Retention time and dispersion associated with submerged aquatic canopies. *Water Resources Research*, 43(4), 1–10. <https://doi.org/10.1029/2006WR005362>
- Nepf, H. M., Mugnier, C. G., & Zavistoski, R. A. (1997). The effects of vegetation on longitudinal dispersion. *Estuarine, Coastal and Shelf Science*, 44(6), 675–684. <https://doi.org/10.1006/ecss.1996.0169>
- Nepf, H. M., Sullivan, J. A., & Zavistoski, R. A. (1997). A model for diffusion within emergent vegetation. *Limnology & Oceanography*, 42(8), 1735–1745. <https://doi.org/10.4319/lo.1997.42.8.1735>
- Nizzetto, L., Bussi, G., Futter, M. N., Butterfield, D., & Whitehead, P. G. (2016). A theoretical assessment of microplastic transport in river catchments and their retention by soils and river sediments. *Environmental Science: Processes & Impacts*, 18(8), 1050–1059. <https://doi.org/10.1039/c6em00206d>
- Ockelford, A., Cundy, A., & Ebdon, J. E. (2020). Storm response of fluvial sedimentary microplastics. *Scientific Reports*, 10, 1–10. <https://doi.org/10.1038/s41598-020-58765-2>
- Peeken, I., Primpke, S., Beyer, B., Gütermann, J., Katlein, C., Krumpen, T., et al. (2018). Arctic sea ice is an important temporal sink and means of transport for microplastic. *Nature Communications*, 9(1), 1–12. <https://doi.org/10.1038/s41467-018-03825-5>
- Poggi, D., Porporato, A., Ridolfi, L., Albertson, J. D., & Katul, G. G. (2004). The effect of vegetation density on canopy sub-layer turbulence. *Boundary-Layer Meteorology*, 111(3), 565–587. <https://doi.org/10.1023/B:BOUN.0000016576.05621.73>
- Rillig, M. C., Lehmann, A., de Souza Machado, A. A., & Yang, G. (2019). Microplastic effects on plants. *New Phytologist*, 223(3), 1066–1070. <https://doi.org/10.1111/nph.15794>
- Rowley, K. H., Cucknell, A. C., Smith, B. D., Clark, P. F., & Morritt, D. (2020). London's river of plastic: High levels of microplastics in the Thames water column. *Science of the Total Environment*, 740, 740. <https://doi.org/10.1016/j.scitotenv.2020.140018>
- Rutherford, J. C. (1994). *River mixing*. John Wiley and Sons.
- Salauddin, M., O'Sullivan, J. J., Abolfathi, S., & Pearson, J. M. (2021). Eco-engineering of seawalls—An opportunity for enhanced climate resilience from increased topographic complexity. *Frontiers in Marine Science*, 8(June), 1–17. <https://doi.org/10.3389/fmars.2021.674630>
- Sana, S. S., Dogiparthi, L. K., Gangadhar, L., Chakravorty, A., & Abhishek, N. (2020). Effects of microplastics and nanoplastics on marine environment and human health. *Environmental Science and Pollution Research*, 27(36), 44743–44756. <https://doi.org/10.1007/s11356-020-10573-x>
- Shucksmith, J. D., Boxall, J. B., & Guymer, I. (2011). Determining longitudinal dispersion coefficients for submerged vegetated flow. *Water Resources Research*, 47(10), 1–13. <https://doi.org/10.1029/2011WR010547>
- Siegfried, M., Koelmans, A. A., Besseling, E., & Kroeze, C. (2017). Export of microplastics from land to sea. A modelling approach. *Water Research*, 127, 249–257. <https://doi.org/10.1016/j.watres.2017.10.011>
- Talsness, C. E., Andrade, A. J. M., Kuriyama, S. N., Taylor, J. A., & Saal, F. S. V. (2009). Components of plastic: Experimental studies in animals and relevance for human health. *Philosophical Transactions of the Royal Society B: Biological Sciences*, 364(1526), 2079–2096. <https://doi.org/10.1098/rstb.2008.0281>
- Taylor, G. (1954). The dispersion of matter in turbulent flow through a pipe. *Proceedings of the Royal Society of London: Series A Mathematical and Physical Sciences*, 223(1155), 446–468. <https://doi.org/10.1098/rspa.1954.0130>
- UK Centre for Ecology and Hydrology. (2021). UK Centre for Ecology and hydrology. Retrieved from <https://www.ceh.ac.uk/future-flows-river-flow-changes-season>
- van Emmerik, T., & Schwarz, A. (2019). Plastic debris in rivers. *Wiley Interdisciplinary Reviews: Water*, 7(1), 1–24. <https://doi.org/10.1002/wat2.1398>
- Vuik, V., Jonkman, S. N., Borsje, B. W., & Suzuki, T. (2016). Nature-based flood protection: The efficiency of vegetated foreshores for reducing wave loads on coastal dikes. *Coastal Engineering*, 116, 42–56. <https://doi.org/10.1016/j.coastaleng.2016.06.001>
- Wagner, M., Christian, S., Diana, A.-M., Nicole, B., Xavier, B., Sebastian, B., et al. (2014). Microplastics in freshwater ecosystems: What we know and what we need to know. *Environmental Sciences Europe*, 26, 1–12. <https://doi.org/10.1186/s12302-014-0012-7>
- Waldschläger, K., Brückner, M. Z. M., Carney Almroth, B., Hackney, C. R., Adyel, T. M., Alimi, O. S., et al. (2022). Learning from natural sediments to tackle microplastics challenges: A multidisciplinary perspective. *Earth-Science Reviews*, 228(April), 104021. <https://doi.org/10.1016/j.earscirev.2022.104021>
- Wallis, S. G., Young, P. C., & Beven, K. J. (1989). Transport in stream channels. *Proceedings - Institution of Civil Engineers*, 87(1)(May), 1–22. <https://doi.org/10.1680/jicp.1989.1450>

- Wang, X., Bolan, N., Tsang, D. C. W., Sarkar, B., Bradney, L., & Li, Y. (2021). A review of microplastics aggregation in aquatic environment: Influence factors, analytical methods, and environmental implications. *Journal of Hazardous Materials*, 402(July 2020), 123496. <https://doi.org/10.1016/j.jhazmat.2020.123496>
- Zhang, W., Mu, S. S., Zhang, Y. J., & Chen, K. M. (2012). Seasonal and interannual variations of flow discharge from Pearl River into sea. *Water Science and Engineering*, 5(4), 399–409. <https://doi.org/10.3882/j.issn.1674-2370.2012.04.004>